

# SplitLab: A shear-wave splitting environment in Matlab<sup>☆</sup>

Andreas Wüstefeld<sup>a,\*</sup>, Götz Bokelmann<sup>a</sup>, Christophe Zaroli<sup>b</sup>, Guilhem Barruol<sup>a</sup>

<sup>a</sup>*Geosciences Montpellier, CNRS, Université de Montpellier II, 34095 Montpellier, France*

<sup>b</sup>*Ecole et Observatoire des Sciences de la Terre, Université Louis Pasteur, Strasbourg, France*

Received 9 November 2006; received in revised form 7 March 2007; accepted 22 August 2007

---

## Abstract

We present a graphical user interface to facilitate the processing of teleseismic shear-wave splitting observations. In contrast to a fully automated technique, we present a manual, per-event approach that maintains user control during the sequence of processing. The SplitLab environment is intended to undertake the repetitive processing steps while enabling the user to focus on quality control and eventually the interpretation of the results. Pre-processing modules of SplitLab create a database of events and link the corresponding seismogram files. The seismogram viewer tool uses this database to perform the measurement interactively. Post-processing of the combined results of such a project includes a viewer and export option. Our emphasis lies in the application to teleseismic shear-wave splitting analysis, but our code can be extended easily for other purposes. SplitLab can be downloaded at <http://www.gm.univ-montp2.fr/splitting/>.

© 2007 Elsevier Ltd. All rights reserved.

**Keywords:** Matlab; Shear-wave splitting; GUI; Seismology

---

## 1. Introduction

Since the early 1990s shear-wave splitting measurements are widely applied to seismological datasets for detecting anisotropy in the Earth (e.g., Vinnik et al., 1989; Silver and Chan, 1991; Silver, 1996; Savage, 1999; Barruol and Hoffmann, 1999; Currie et al., 2004; Walker et al., 2005; Heintz and Kennett, 2006). While seismic anisotropy in the upper crust is primarily controlled by preferred orientations of microcracks (e.g., Crampin and Chastin, 2003), it is dominated in the deeper Earth, and particularly in the upper mantle, by the

preferred orientation of anisotropic crystals (e.g., Tommasi, 1998).

Similar to birefringence in optics, shear-wave splitting occurs whenever a seismic shear-wave travels through an anisotropic layer. It is split into two waves propagating at different speeds, which are polarized in two perpendicular orientations (Fig. 1): one wave is polarized along the seismic fast axis direction and the other perpendicular, along the seismic slow axis direction. The delay time measured at the Earth's surface between the two split waves depends on the strength of anisotropy and on the thickness of the anisotropic layer.

Seismic anisotropy has been observed in many environments and at many depths in the Earth, from the crust down to the core–mantle boundary (CMB). In the upper mantle, anisotropy is a common feature and isotropy is rather the exception. Anisotropy is

---

<sup>☆</sup> Code available from server at <http://www.iamg.org/CGEditor/index.htm>

\*Corresponding author.

E-mail address: [splitlab@gmx.net](mailto:splitlab@gmx.net) (A. Wüstefeld).



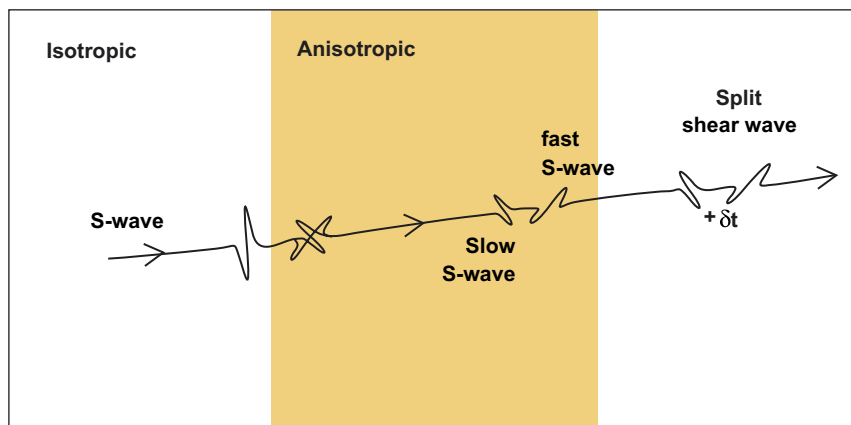


Fig. 1. Shear-wave splitting occurs for a shear wave traveling through an anisotropic medium (shaded). When incident shear wave arrives at an anisotropic medium, it splits into two shear waves of perpendicular polarization, along seismic fast and slow directions, respectively. Traveling through anisotropic medium, the two waves accumulate a delay time  $\delta t$ . Shear-wave splitting techniques invert for  $\delta t$  and the fast polarization direction  $\Phi$ .

widely accepted to be directly related to mantle deformation aligning rock-forming crystals that are intrinsically anisotropic. Measuring anisotropy remotely from the Earth's surface is therefore a way to access present or past mantle flow at depth. Anisotropy thus offers the unique possibility to directly observe and measure Earth's properties and geodynamic processes at depth. In order to characterize this upper mantle anisotropy, core shear phases such as SKS and SKKS are generally used. These phases are well detectable at distances between  $90^\circ$  and  $130^\circ$  from the epicenter. They propagate along steeply inclined rays between the core and the surface, while the liquid nature of the outer core and the P-to-S conversion at the CMB ensures that only receiver-side splitting is observed. Reviews of the shear-wave splitting technique and its applications have been given by Silver (1996) and Savage (1999).

A number of codes for performing teleseismic shear-wave splitting measurements exist in the community. Generally, these consist of combinations of FORTRAN, C, or C++ programs, which are embedded in SAC, SeismicUnix, or Seismic-Handler scripts. Such a “command line approach” is feasible for small amounts of data. However, more data have become available during the last decade, due to the increasing number of stations from both temporary and permanent networks (like GSN, IRIS, Geoscope, and GEOFON amongst others). To efficiently analyze and interpret these growing datasets, we present the new SplitLab processing environment. Splitlab is available for

free download at <http://www.gm.univ-montp2.fr/splitting>. With its intuitive “button approach”, we aim to provide a modern, efficient, flexible, and user-friendly workflow (Fig. 2). Based on Matlab, this environment is platform independent. A set of *graphical user interfaces* (GUIs) embraces the entire splitting workflow, including the selection of appropriate earthquakes and data requests in various formats. Furthermore, a seismogram viewer is provided for selection of the relevant phase window and the resulting splitting diagnostic plots. The process for a single station is saved as a ‘Project’, providing for the possibility to conduct multiple analyses on the same data set, to resume work at a later time, or for the easy exchange of data between researchers.

SplitLab is designed and tested for the use of SKS phases in three-component records in SAC format of permanent stations. However, the shear-wave splitting analysis of other phases, such as direct S or ScS, and the analysis of temporary networks are also possible.

## 2. Modules description

The SplitLab workflow (Fig. 2) can be divided into several steps: (1) configuration of the project, data request, and database preparation, (2) seismogram validation and shear-wave splitting procedure, and (3) results output and analysis. At each step the database can be accessed with an integrated viewer,



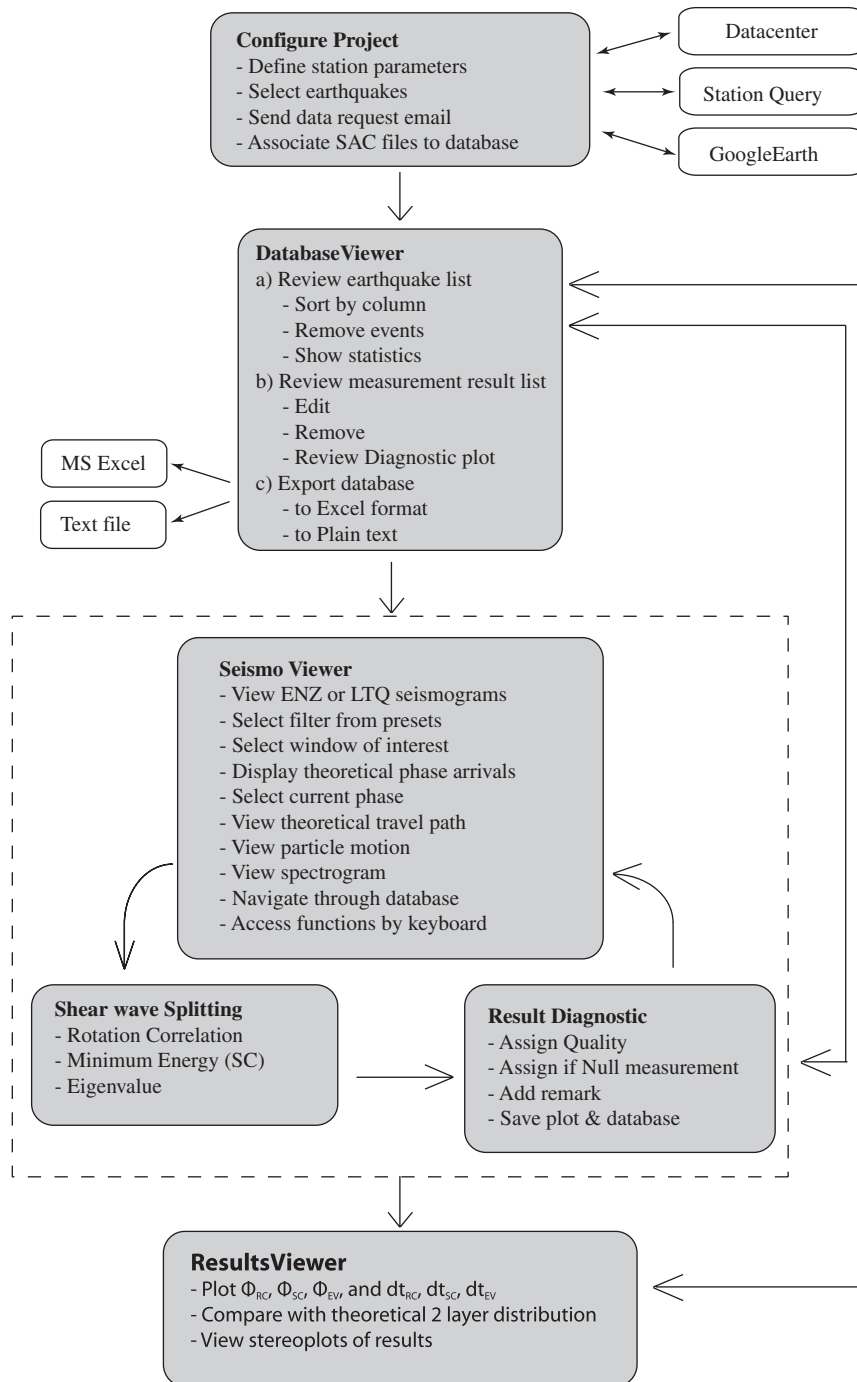


Fig. 2. SplitLab workflow with descriptions of each module.

which also comprises an export option to Microsoft Excel or plain text format.

A SplitLab project consists of the two Matlab-Structure variables “config” and “eq”. Such a

format eases the extension of SplitLab with any future plug-ins or interaction with user functions. The “config” structure contains fields with general project configuration (file locations, event search,



station parameters, etc.) and the “eq” structure contains the earthquake database (e.g., location, magnitude, distance, corresponding SAC files, results, etc.). See Appendixes B and C for the actual information stored in the structures. A detailed description of the variable-type “structure” is provided in the Matlab manual.

### 2.1. The SplitLab Project configuration (*splitlab.m*)

To create and manage a SplitLab Project, we provide a GUI (Fig. 3) where the user can set up the parameters of the project. After entering information concerning the station, the user can choose between the Harvard CMT catalog and the NEIC catalog for selecting the earthquake window (time period, distance, magnitude, and depth). A statistical plot provides graphical information about the earthquakes matching the given criteria (Fig. 4). Both catalogs exist as local files, and an updater helps to download the newest earthquakes from the corresponding web pages (Fig. 3).

At this point, SplitLab requires the presence of waveforms on the local computer. SplitLab allows the waveforms to be requested from different data

centers via email in various formats such as AutoDRM, BreqFast, netDC, or saved as a plain text table. In case the SAC files are already accessible to the user (old analysis, local/temporary deployments), this request step can be omitted. Once the data centers have provided the seismograms and these are converted to SAC format, the “Find Files” panel allows searching for and linking the three files (east, north, and vertical components) to the corresponding earthquake entry of the database. This is done by comparing, within a variable search tolerance, the hypocentral time in the catalogue with the start time of the seismogram file as provided by the filename or its header values. A static offset time can also be selected if, for example, the seismograms are provided relative to P-wave arrival. At the same time, phase arrival times of various seismic phases are calculated and added to the database. This processing step is explained in more detail in the Appendix D.

### 2.2. The seismogram viewer

The main environment of the shear-wave splitting procedure is the Seismogram Viewer. Here, the

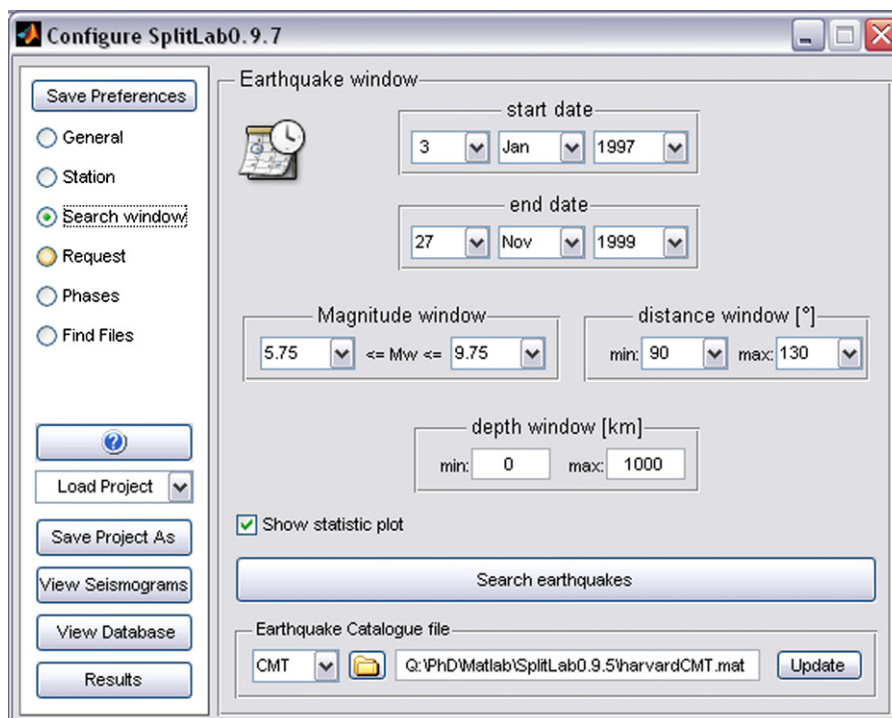


Fig. 3. Configuration of SplitLab can be accessed interactively. Here, for example, the earthquake window selection panel.



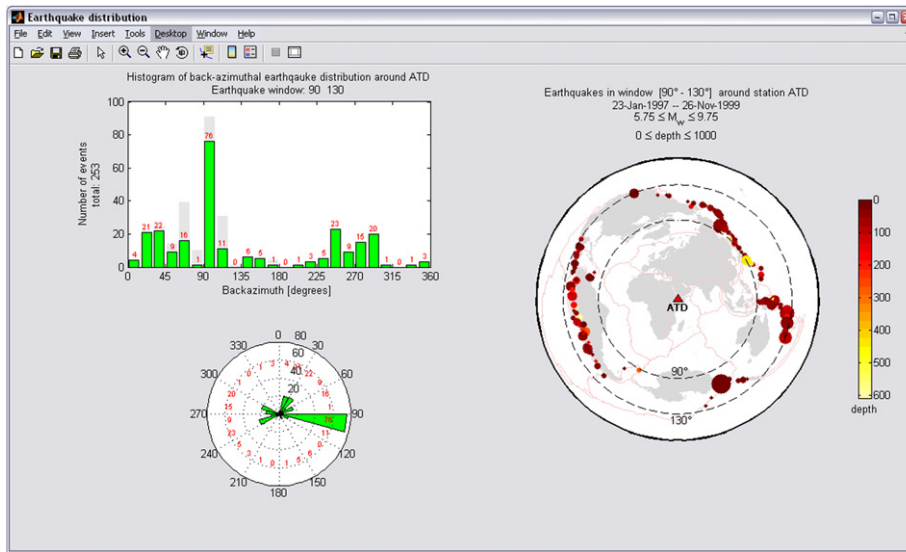


Fig. 4. Earthquake distribution statistic plot. The upper left displays backazimuthal distribution as histogram in  $15^\circ$  bins (displayed in gray are cumulated earthquakes within these bins for  $180^\circ$  periodicity). The lower left is same displayed in a rose plot. The right panel gives an equidistant azimuthal map of earthquake locations.

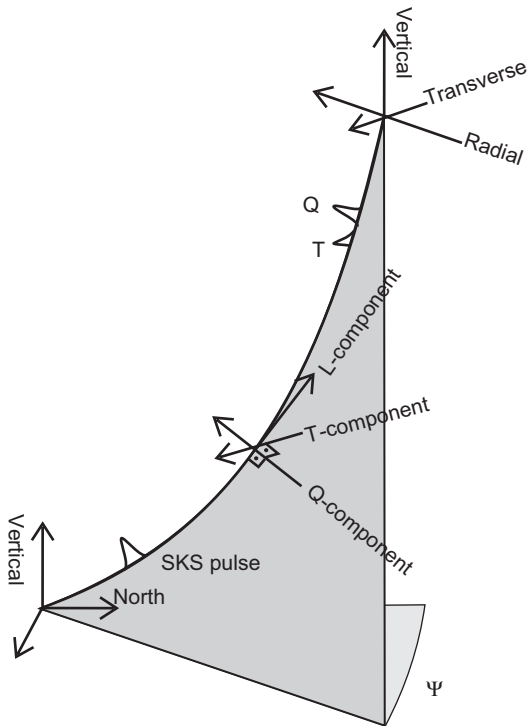


Fig. 5. Components of a seismogram in a right-handed L-Q-T system. Ray plane, shown in gray, is given by L-component (pointing along ray from earthquake towards station) and Q-component (pointing towards earthquake). T-component is perpendicular to this ray plane.  $\Psi$  is backazimuth.

seismograms are read and stored in the temporary structure variable “thiseq”, together with the corresponding earthquake parameters. Furthermore, a rotation into the three-dimensional ray system (LQT, Fig. 5) is performed:

$$\begin{bmatrix} L \\ Q \\ T \end{bmatrix} = \begin{bmatrix} \cos \delta & -\sin \delta \sin \beta & -\sin \delta \cos \beta \\ \sin \delta & \cos \delta \sin \beta & \cos \delta \cos \beta \\ 0 & -\cos \beta & \sin \beta \end{bmatrix} \cdot \begin{bmatrix} Z \\ E \\ N \end{bmatrix},$$

where  $\beta$  is the backazimuth (positive clockwise from north) and  $\delta$  is the incidence angle of the wave, measured from vertical ( $\delta = 0^\circ$  for vertically incident waves;  $\delta = 90^\circ$  for horizontally incident waves; Plesinger et al., 1986). In this case, the positive (longitudinal) L-component points along the ray path (from the earthquake towards the station), and the Q-component is defined as positive when pointing towards the earthquake (Fig. 5). The T-component completes the right-handed coordinate system. The incidence angle of each phase is calculated from the ray path function of the matTaup toolbox, which is automatically installed with the Matlab toolboxes during the SplitLab installation. By default, SplitLab displays the LQT-seismograms for the incidence angle of the SKS phase, but this can be changed easily in the phase selector menu in the bottom panel of



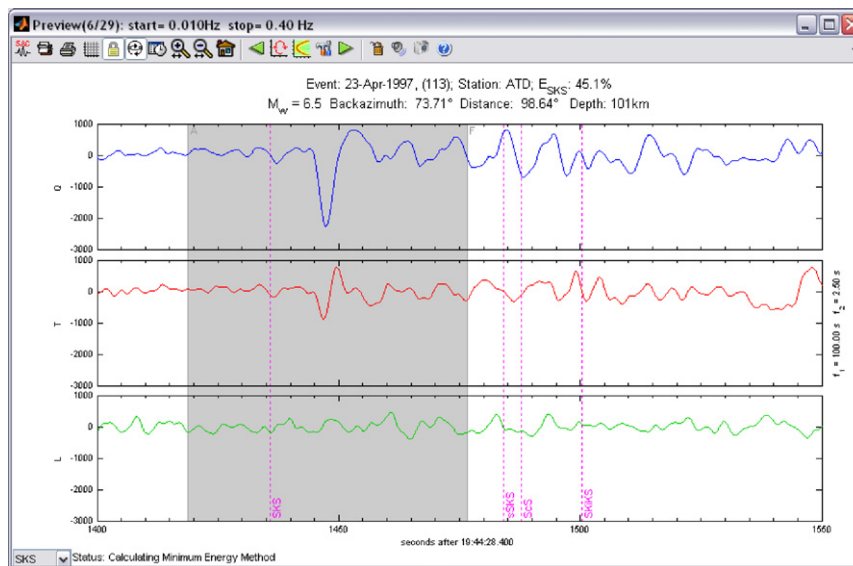


Fig. 6. The Seismogram viewer with selected window (shaded area). Various menu buttons provide display options and navigation within SplitLab database. Phase of interest can be selected by a menu in lower left corner.

the Seismogram Viewer (Fig. 6). This feature can also be used to differentiate between close phase arrivals, e.g. the SKS and the SKKS phases, which should have different energies on the L-component when rotated with the appropriate incidence angle.

Within the Seismogram Viewer environment, the waveforms can be visually inspected and analyzed by the user before shear-wave splitting measurements. Functions such as rotations, filters, zooms, particle motion analyses, and spectrograms are easily accessible to help the user in the selection of the seismic phase and of the time selection for further measurements. Several keyboard keys serve as direct access to functions (Table 1). For example, the keys “0”–“9” provide a suite of preset frequency filters, which apply a third-order Butterworth filter twice to produce zero-phase distortion. Pressing the “Home” key zooms directly to the selected phase. The users can easily add key-press functions by changing the file `seisKeyPress.m`. Additional features include a particle motion viewer and an export to SAC format of the current view. The time window on which the user wishes to perform a splitting measurement is selected by mouse clicks.

### 2.3. The shear-wave splitting measurement

The effect of shear-wave splitting occurs when an S-wave propagates through an anisotropic layer

Table 1

Keyboard presets of SplitLab’s Seismogram viewer

Key	Function
f	Open filter dialog
0	Unfiltered data
1	0.01–0.1 Hz
2	0.02–0.2 Hz
3	0.02–0.3 Hz
4	0.01–0.3 Hz
5	0.01–0.4 Hz
6	0.02–1 Hz
7	0.01–0.15 Hz
8	0.02–0.25 Hz
9	0.01–1 Hz
+	Add 0.002 Hz to lower filter frequency
–	Subtract 0.002 Hz from lower filter frequency
*	Add 0.02 Hz to upper filter frequency
/	Subtract 0.002 Hz from upper filter frequency
Space	Switch between ZEN and LQT system
Backspace	Reset zoom state
PageUp	Scroll right
PageDown	Scroll left
Home	Zoom to phase
Enter	Start shear-wave splitting

These can be changed or supplementary functions can be added in script `seisKeyPress`.

(Fig. 1). The wave is split into two shear waves, polarized in the fast and slow directions and accumulating a delay time along their paths (e.g.,



Savage, 1999). To remove the effect of splitting (and thus find the fast direction and delay time), SplitLab uses simultaneously three different techniques. The first is the rotation–correlation method (hereafter RC; e.g., Bowman and Ando, 1987), the second is the minimum energy method (hereafter SC; Silver and Chan, 1991), and the third is the eigenvalue method (EV; e.g., Silver and Chan, 1991). The SC technique can be seen as a special case of the EV technique, and may be applied if, as for the SKS phase, the initial polarization of the wave is known. All three techniques perform a grid-search for the splitting parameters  $\Phi$  (fast axis) and  $\delta t$  (delay time), which best remove the effect of splitting, that is, linearize the particle motion in either the E–N or the Q–T plane. As a criterion for best linearization,

the RC technique uses the maximization of the cross-correlation coefficient between the waveforms on the radial Q and transverse T components in the selected window. The SC technique searches for the minimum energy of displacement  $u_T$  on the transverse component ( $E = \sum u_T^2$ ). Silver and Chan (1991) point out the similarities between the four eigenvalue-based criteria such as maximizing  $\lambda_1$  or  $\lambda_1/\lambda_2$ , and minimizing  $\lambda_2$  or  $\lambda_1*\lambda_2$ . The user of SplitLab can choose between either of these criteria.

The initial polarization of the wave is assumed to be radial in the case of the RC and SC methods, which are thus only applicable to phases such as SKS, SKKS, PKS, etc. For the EV method, SplitLab provides the option to either use the backazimuth as initial polarization or to estimate

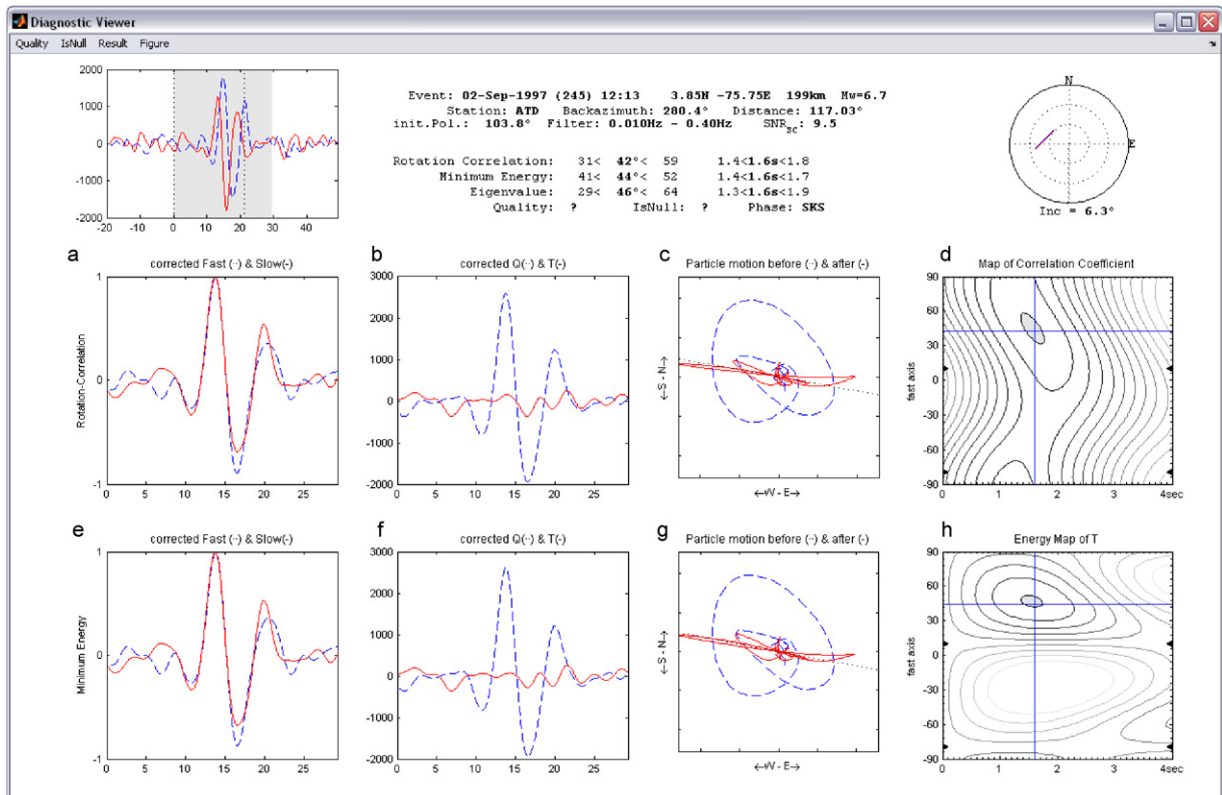


Fig. 7. Diagnostic plot of a single measurement. Center panels displays result for the rotation–correlation (RC) technique: (a) seismogram components in fast (solid) and slow (dashed) directions for RC-anisotropy system after RC-delay correction (normalized); (b) radial (Q, solid) and transverse (T, dashed) components after RC-correction (not normalized); (c) particle motion before (dashed) and after (solid) RC correction; and (d) map of correlation coefficients. Lower panels display results for the minimum energy (SC) technique: (e) seismograms shown after splitting correction shown on SC fast and slow components (normalized); (f) same on radial and transverse components (not normalized); (g) SC particle motion before and after correction; (h) map of minimum energy values on transverse component. In upper left panel an extended section of Q (solid) and T (dashed) components before anisotropy correction is displayed. In upper right panel a stereoplot of the result is presented. Header gives specifications of event as well as splitting parameters resulting from three techniques. Depending on the chosen option, the lower panels (e)–(h) may display instead of SC the results of the EV technique.



it from the particle motion after anisotropy correction and linearization of the waveform. The latter should be used for phases where the initial polarization is unknown (direct S, ScS, etc.).

The default search grid parameters used in SplitLab are steps of  $1^\circ$  and half the sampling rate for the RC technique and  $2^\circ$  and half the sampling rate for the SC and EV techniques, respectively. The determination of the error is discussed in Appendix A.

For all these calculations the original seismograms are used, which are tapered on both ends. Any existing linear trend is removed from the traces, the mean is subtracted, and finally the whole trace is filtered. Then the seismograms are cut according to the picks. The selection window is extended by 30 s before and after the picks and inserted into the splitting calculation routines. The results of these calculations are displayed in a diagnostic plot (Fig. 7) containing several graphics, allowing the user to quickly visualize and evaluate the measurement. The quality of the measurement can be assigned as proposed by Barruol et al. (1997) via a menu or the measurement can be discarded to test another time

window, another filter, another seismic phase, or another seismic event. An optional remark on each measurement can also be added to the database.

#### 2.4. The database viewer

The database of a SplitLab project can easily be accessed with the database viewer. A table of the events displays some necessary information. Here, the user can sort the event list, for example by backazimuth, depth, distance, or magnitude. Selecting one or more events displays the results of previously performed splitting measurements in the lower panel of the database viewer. By selecting one result, a direct access to the corresponding diagnostic plot is possible and allows the user to easily manage previous measurements. Furthermore, the results of the project can be exported in Excel format or as plain text for further analysis.

#### 2.5. The result viewer

The results of a project can finally be presented by the Result Viewer module (Fig. 8). The user can

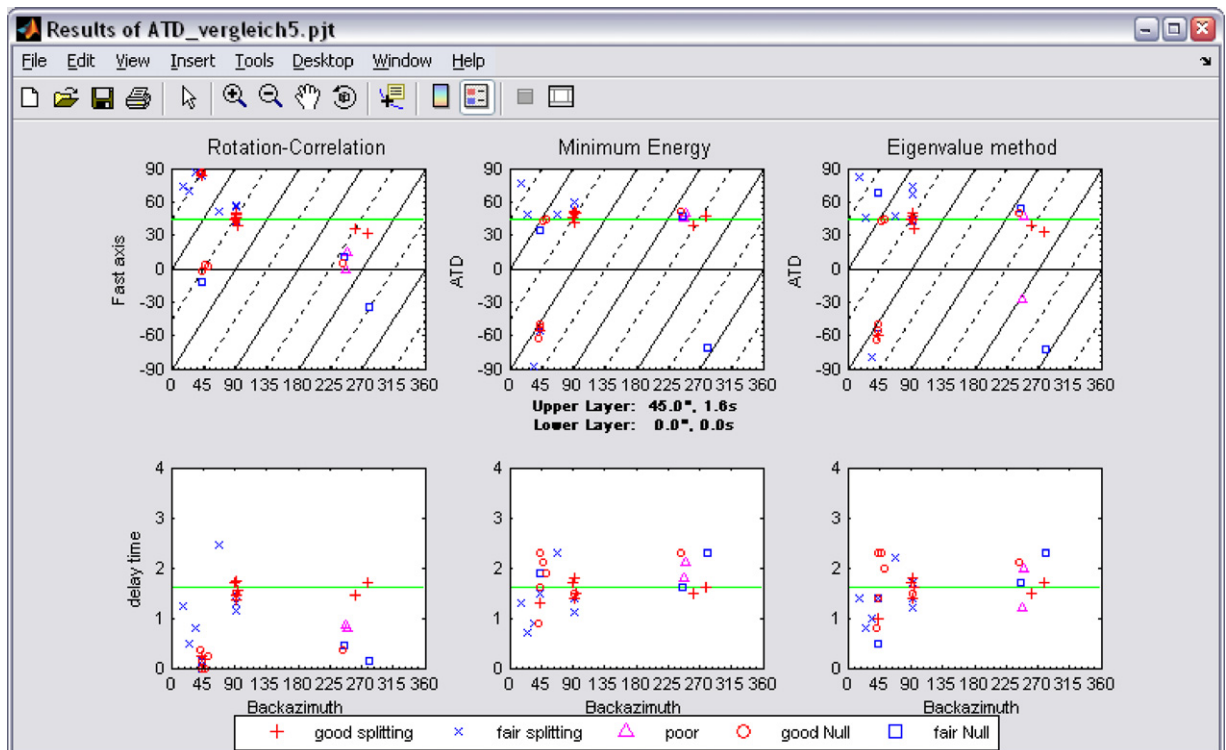


Fig. 8. Results of splitting project for station ATD. Horizontal lines indicate one-layer solution with parameters  $\Phi = 48^\circ$  and  $\delta t = 1.6$  s.



interactively choose the desired phases and qualities to be displayed in the plot. The backazimuthal variation of fast axis estimates and delay time estimates of the RC, SC, and EV methods are plotted. Such a variation may provide evidence, if any, of the presence of several anisotropic layers beneath the station. In addition, the theoretical backazimuthal distribution of the apparent splitting parameters for two layers of anisotropy can be calculated and plotted (Savage and Silver, 1994). This allows the user to interactively test numerous models and to visualize their fit to the observations.

### 3. Validation

The SplitLab environment has been tested and validated through synthetic tests, but also by analyzing real data that were already processed and published by different authors.

#### 3.1. Synthetic tests

We performed synthetic tests to compare the accuracy and behavior of the different splitting techniques. Wüstefeld and Bokermann (2007) explain the results of these tests in detail. In summary, they find that both the RC and SC techniques reconstitute input fast axes and delay times very well at different noise levels for backazimuths far from input fast and slow axes, where the energy on the transverse component is large. The higher the signal-to-noise ratio, the wider the backazimuthal range of reliable splitting parameter estimates.

However, at backazimuths close to fast and slow axes (“null directions”), the RC and SC techniques yield characteristic differences. There, the fast axes estimates of the RC technique deviate  $45^\circ$  from the input fast axis, while the fast axis estimates from the SC technique,  $\Phi_{SC}$ , scatter around either the correct fast or the slow axis orientation. The RC delay time estimates,  $dt_{RC}$ , tend towards small values, close to 0 s, while  $dt_{SC}$  shows large scattering with values above 0.5 s and often close to the maximum allowed by the grid search.

The backazimuth range of good estimates is larger for the SC than for the RC technique. These characteristic differences can be used to identify nulls in real datasets and to assign a quality to the measurement. Not explicitly discussed in Wüstefeld and Bokermann (2007) is the behavior of the various

eigenvalue methods. These show, however, similar results to the SC method in the synthetic test.

#### 3.2. Validation on real data: the Geoscope station ATD

We provide with SplitLab a data example from the Geoscope station ATD (Arta Cave, Djibouti). The choice of this station has been guided by the quality of the data, the clarity of the fast azimuth, the strength of the delay time, and the broad agreement on the splitting parameters obtained from various anisotropy studies previously performed and published at this station (Vinnik et al., 1989; Barruol and Hoffmann, 1999) and also at neighboring stations (e.g., Ayele et al., 2004; Gashawbeza et al., 2004).

The example SplitLab project file contains the necessary parameters and associations, so that the user can directly test the program. Within the provided SAC files, we set the A and F header variables that mark the beginning and end of the time window, respectively. These markers are plotted in the Seismogram Viewer and thus hint an inexperienced user to the best time window selection. The selection itself, however, still has to be done. The splitting parameters obtained from the three methods provided in SplitLab are presented in Table 2 together with the results of Barruol and Hoffmann (1999), performed on the same dataset by using the SC method. Our results are in very good agreement with theirs. Except for a few events of fair or poor quality, the observed difference falls within  $\pm 3^\circ$  for the azimuth  $\phi$  of the fast split shear wave and within  $\pm 0.20$  s for the delay times. For the measurements qualified as “good” by Barruol and Hoffmann (1999), the agreement generally falls, respectively, within  $\pm 3^\circ$  and  $\pm 0.05$  s. The SplitLab results obtained by using the SC and EV method are similar, indicating for station ATD splitting parameters of  $\Phi = 45^\circ$  and  $\delta t = 1.6$  s. For the non-null measurements, the difference is generally less than  $3^\circ$  between the azimuth and less than 0.2 s for the delay times. The RC method compares fairly well for the “good” measurements with the SC method but, for “fair” and “poor” quality measurements, displays large differences in some cases up to  $45^\circ$  in azimuth. As demonstrated by Wüstefeld and Bokermann (2007), a useful application of the RC method is for distinguishing true nulls from small delay times in the case of noisy records.



Table 2

Anisotropy parameter estimates for station ATD by Barruol and Hoffmann (1999) and SplitLab. Barruol and Hoffman used the SC technique to obtain the splitting parameters, so a direct comparison is only possible to this technique, marked in gray

Event	Phase	Barruol and Hoffmann (1999)			Splitlab 2006						$\Delta\Phi$	$\Delta dt$
		$\phi$	$dt$	Quality	$\Phi$ RC	$\Phi$ SC	$\Phi$ EV	$dt$ RC	$dt$ SC	$dt$ EV		
<i>Good</i>												
93.286	SKS	50	1.35	g	49	51	51	1.40	1.40	1.40	1	0.05
93.289	SKS	48	1.50	g	43	49	48	1.50	1.50	1.50	1	0.00
93.298	SKS	48	1.45	g	48	49	48	1.50	1.40	1.40	1	0.05
94.157	SKS	47	1.60	g	31	47	49	1.70	1.60	1.70	0	0.00
94.289	SKS	−61	0.95	g	85	−62	−62	0.40	0.90	0.80	1	0.05
95.079	SKS	47	1.50	g	39	50	41	1.60	1.50	1.60	3	0.00
95.122	SKS	44	1.65	g	44	44	38	1.70	1.70	1.80	0	0.05
95.175	SKS	46	1.70	g	44	46	47	1.70	1.70	1.70	0	0.00
95.175	SKKS	49	1.70	g	49	50	50	1.60	1.50	1.50	1	0.20
95.353	SKS	42	1.80	g	47	42	42	1.80	1.70	1.70	0	0.10
96.162	SKS	48	0.70	g	69	49	45	0.50	0.70	0.90	1	0.00
<i>Fair</i>												
93.192	SKS	47	1.95	f	−1	45	3	0.90	1.80	1.20	2	0.15
94.010	SKS	35	1.35	f	37	38	38	1.50	1.50	1.50	3	0.15
94.362	SKS	44	2.35	f	3	42	41	0.10	2.90	2.30	2	0.55
95.226	SKS	58	1.30	f	56	59	63	1.30	1.40	1.70	1	0.10
95.337	SKS	−55	1.40	f	86	−53	−55	0.20	1.60	1.40	2	0.20
96.047	SKS	44	2.05	f	2	44	44	0.30	1.90	1.90	0	0.15
96.053	SKS	−53	1.65	f	84	−55	−56	0.30	1.30	1.00	2	0.35
96.128	SKS	−53	1.45	f	82	−56	−53	0.10	1.50	1.50	3	0.05
<i>Poor</i>												
93.323	SKS	82	1.40	p	68	74	76	1.20	1.10	1.20	8	0.30
94.108	SKS	54	1.10	p	49	56	60	1.10	1.20	1.30	2	0.10
94.231	SKS	44	1.20	p	11	47	45	0.50	1.60	1.70	3	0.40
95.211	SKS	51	2.00	p	14	50	51	0.80	2.10	2.00	1	0.10
95.235	SKS	49	2.20	p	52	49	48	2.50	2.30	2.10	0	0.10
95.305	SKS	52	2.30	p	4	51	53	0.40	2.30	2.10	1	0.00
96.120	SKS	49	1.45	p	40	48	49	1.40	1.50	1.40	1	0.05
<i>Null</i>												
95.118	SKS	−47	4.00	g	−2	−50	−49	0.00	2.30	2.20	3	1.70
96.038	SKS	40	4.00	g	−12	34	78	0.00	2.10	0.00	6	1.90

Last two columns represent difference in fast axis estimates ( $\Delta\Phi$ ) and delay time estimates ( $\Delta\delta t$ ) between Barruol and Hoffmann (1999) and SplitLab results of the SC technique.

#### 4. Conclusions

We have presented a code that performs shear-wave splitting measurements including the entire workflow from pre-processing to data analysis to resulting diagnostics. The SplitLab environment provides an efficient approach to the interactive processing and managing of large seismological datasets. Different from other recent approaches (Teanby et al., 2003; Evans et al., 2006), our aim is not to fully automate the whole process. Instead, the

chosen interactive approach allows the user to focus on the critical steps such as event selection, quality control, and phase picking, while the computer undertakes less important and repetitive aspects of processing. Based on Matlab, SplitLab is system-independent and directly portable to different operating systems. It has been successfully tested on Windows, MAC, and Linux systems. The simultaneous evaluation of three different splitting techniques provides for the maximum information to be obtained from a single measurement.



We encourage users to contact us on modifications they propose to the original code or additional plug-ins. This should enable SplitLab to change and grow dynamically, in the spirit of the General Public License.

## Acknowledgments

We thank M. Savage, S. Greve and C. Currie for helpful comments that improved our manuscript. We are grateful to Alexander Gatzemeier, Luisa Buontempo and Sonja Greve for their patience and helpful ideas as test users of earlier versions. Extensive use is made of the SACLAB toolbox by Michael Thorne (<http://gcc.asu.edu/mthorne/saclab/>) for incorporating the SAC files to Matlab and the matTaup toolbox by Qin Li (<http://www.ess.washington.edu/SEIS/FMI/matTaup.htm>) to calculate the phase arrivals. Finally, we would like to thank Véronique Le Roux for the SplitLab logo.

## Appendix A. Error calculation

We calculate the error of the SC and the EV techniques following Silver and Chan (1991). In their approach, the energy  $E(\phi, dt) = \sum u_T^2(\phi, dt)$  on the transverse component  $u_T$  for a test fast axis  $\Phi$  and test delay time  $dt$  is assumed to be  $\chi^2$ -distributed variable with  $n$  degrees of freedom. This assumes a Gaussian noise process, for which the number of degrees of freedom can be estimated from the seismogram. We then estimate the confidence region of  $\Phi$  and  $dt$  that corresponds to

$2\sigma$ . We use as error bounds the minimum and maximum range of the confidence region, in contrast to the (systematically smaller) marginal error that is often applied.

To obtain error information for the rotation–correlation technique, one can either relate the correlation coefficient to the sum-of-squares (Bokelmann, 1992), or use the Fisher transformation (Fisher, 1925). The latter transforms the (normalized) correlation coefficient  $r$  to an approximately Gaussian distribution. We illustrate here the Fisher transformation approach:

Let

$$z = \operatorname{arctanh}(r) = \frac{1}{2} \log \left( \frac{1+r}{1-r} \right),$$

where  $z$  is a parameter representing the transformed correlation coefficient. Then, as  $r$  changes from 0 to 1,  $z$  will pass from 0 to infinity. For small values of  $r$ ,  $z$  is nearly equal to  $r$ , but as  $r$  approaches unity,  $z$  increases without limit. For negative values of  $r$ ,  $z$  is negative. The distribution of  $z$  is not strictly normal, but it tends to normality rapidly as the sample number is increased (Fisher, 1925), whatever the value of  $r$ . The distribution  $z$  has a standard deviation of  $\sigma_z = \sqrt{1/n-3}$ , from which we can now calculate the  $2\sigma$ -confidence level  $\mu_z$ .

This value is then transformed back into  $r$ -space, resulting in the  $2\sigma$ -confidence level of the correlation coefficient:

$$\mu_r = \tanh(\mu_z).$$



**Appendix B. Fields of variable “config”**

```

version: 'SplitLab0.9.7'
host: 'SEALAB'
project: 'ATD_example.pjt'
datadir: 'Q:\PhD\_SplitlabExamples\ATD_example'
projectdir: 'Q:\PhD\_SplitlabExamples\'
savedir: 'Q:\PhD\_SplitlabExamples\ATD_example\Results'
calcpase: 1
calcEnergy: 1
showstats: 1
stnname: 'ATD'
netw: 'G'
slat: 11.5300
slong: 42.8470
elev: []
eqwin: [90 130]
z_win: [0 1000]
twin: [3 1 1997 27 11 1999]
Mw: [5.7500 9.7500]
catalogue: 'Q:\PhD\Matlab\SplitLab0.9.7\harvardCMT.mat'
catformat: 'CMT'
searchstr: '*.SAC'
searchdt: 420
offset: 0
request:
    label: 'label'
    format: 'NetDC'
    reqtime: [-60 2400]
    comp: 'BH?'
    user: 'wueste'
    usermail: 'wueste@dstu.univ-montp2.fr'
    institut: 'Institut'
    adress: '99 Example Road, 12345 Mytown, Mycountry'
    phone: ''
    fax: ''
    DataCenters: {5x1 cell}
    mailto: 'netdc@fdns.org'
    timestamp: '24-Jul-2006 16:03:52'

    phases: {1x20 cell}
    earthmodel: 'iasp91'
    exportformat: '.eps'
    comment: [9x88 char]
    db_index: 1
    maxSplitTime: 4
    splitoption: 'Minimum Energy'
    UseHeaderTimes: 0
    rotation: 0
    SwitchEN: 0
    signE: 1
    signN: 1
    FileNameConvention: 'RDSEED'
    PaperType: 'A4'
    tablesortcolumn: 1

```



## Appendix C. Fields of variable “eq”

```

date: [1997 1 23 2 15 22.9000 23]
dstr: '23-Jan-1997'
lat: -22
long: -65.7200
depth: 276
azi: 85.7850
bazi: 250.6860
dis: 111.3551
Mw: 7.1118
M0: 5.7900e+026
meca: [85 4 -175]
region: 'SOUTHERN BOLIVIA'
seisfiles: {3x1 cell}
offset: [3x1 double]
index: [1 1 1]
phase: [1x1 struct]
energy: -0.9336
polarisation: 71.7136
results:
    SplitPhase: 'SKS'
    incline: 6.9695
    quality: 'good'
    Null: 'No'
    filter: [0.0200 1]
    phiRC: [27.6536 38.6860 47.7654]
    dtRC: [1.4000 1.8000 2.2000]
    phiSC: [39.4382 42.6860 49.5506]
    dtSC: [1.7000 1.9000 2.1000]
    phiEV: [39.4382 43.7136 49.5506]
    dtEV: [1.7000 1.9000 2.1000]
    a: 1.4503e+003
    f: 1.5012e+003
    SNR: [4x1 double]
    remark: ''
    method: 'Minimum Energy'
    timestamp: '25-Jul-2006 12:05:55'
    resultplot: '1997.023.02_result_SKS.eps'
    seisplot: '1997.023.02_LTQseismo_SKS..eps'

```

## Appendix D. Supplementary material

Supplementary data associated with this article can be found in the online version at [doi:10.1016/j.cageo.2007.08.002](https://doi.org/10.1016/j.cageo.2007.08.002).

## References

- Ayele, A., Stuart, G., Kendall, J.M., 2004. Insights into rifting from shear wave splitting and receiver functions: an example from Ethiopia. *Geophysical Journal International* 157, 354–362.
- Barruol, G., Hoffmann, R., 1999. Upper mantle anisotropy beneath the Geoscope stations. *Journal of Geophysical Research* 104, 10757–10773.
- Barruol, G., Silver, P.G., Vauchez, A., 1997. Seismic anisotropy in the eastern US: deep structure of a complex continental plate. *Journal of Geophysical Research* 102, 8329–8348.
- Bokelmann, G., 1992. Upper and lower mantle small-scale heterogeneity studied by systematic analysis of portable broadband waveforms and travel times. Ph.D. Dissertation, Princeton University, Princeton, NJ, 197pp.
- Bowman, J.R., Ando, M., 1987. Shear-wave splitting in the upper-mantle wedge above the Tonga subduction zone. *Geophysical Journal of the Royal Astronomical Society* 88, 25–41.
- Currie, C.A., Cassidy, J.F., Hyndman, R.D., Bostock, M.G., 2004. Shear wave anisotropy beneath the Cascadia subduction zone and western North American Craton. *Geophysical Journal International* 157, 341–353.
- Crampin, S., Chastin, S., 2003. A review of shear wave splitting in the crack critical crust. *Geophysical Journal International* 155, 221–240.
- Evans, M.S., Kendall, J.M., Willemann, R.J., 2006. Automated SKS splitting and upper mantle anisotropy beneath the Canadian seismic stations. *Geophysical Journal International* 165, 931.
- Fisher, R.A., 1925. *Statistical Methods for Research Workers*, first ed. Oliver and Boyd, Edinburgh, 239pp.



- Gashawbeza, E.M., Klemperer, S.L., Nyblade, A.A., Walker, K.T., Keranen, K.M., 2004. Shear-wave splitting in Ethiopia: Precambrian mantle anisotropy locally modified by Neogene rifting. *Geophysical Research Letters* 31, L18602.
- Heintz, M., Kennett, B.L.N., 2006. The apparently isotropic Australian upper mantle. *Geophysical Research Letters* 33, L15319.
- Plesinger, A., Hellweg, M., Seidl, D., 1986. Interactive high-resolution polarization analysis of broadband seismograms. *Journal of Geophysics* 59, 129–139.
- Savage, M.K., 1999. Seismic anisotropy and mantle deformation: what have we learned from shear wave splitting. *Reviews of Geophysics* 37, 69–106.
- Silver, P.G., 1996. Seismic anisotropy beneath the continents: probing the depths of geology. *Annual Reviews of Earth Planetary Sciences* 24, 385–432.
- Silver, P.G., Chan, W.W., 1991. Shear wave splitting and subcontinental mantle deformation. *Journal of Geophysical Research* 96, 16429–16454.
- Savage, M.K., Silver, P.G., 1994. The interpretation of shear-wave splitting parameters in the presence of two anisotropic layers. *Geophysical Journal International* 119, 949–963.
- Teanby, N., Kendall, J.M., van der Baan, M., 2003. Automation of shear-wave splitting measurements using cluster analysis. *Bulletin of the Seismological Society of America* 94, 453–463.
- Tommasi, A., 1998. Forward modeling of the development of seismic anisotropy in the upper mantle. *Earth and Planetary Science Letters* 160, 1–13.
- Vinnik, L.P., Farra, V., Romanovicz, B., 1989. Azimuthal anisotropy in the earth from observations of SKS at Geoscope and NARS broadband stations. *Bulletin of the Seismological Society of America* 79, 1542–1558.
- Walker, K.T., Bokelmann, G.H.R., Klemperer, S.L., Bock, G., 2005. Shear-wave splitting around the Eifel hotspot: evidence for a mantle upwelling. *Geophysical Journal International* 163, 962–980.
- Wüstefeld, A., Bokelmann, G., 2007. Null detection and weak anisotropy in shear-wave splitting. *Bulletin of the Seismological Society of America* 97 (4), 1204–1211.